Chemical Physics Letters 803 (2022) 139859

Contents lists available at ScienceDirect

Chemical Physics Letters

journal homepage: www.elsevier.com/locate/cplett

The enhanced dyes removal and catalytic property for nanofused structural chromium-benzenedicarboxylate metal-organic framework

Tian Zhao [a], Wei Geng [a], Ming Dong [d], Yi Zhao [d], Christoph Janiak [c,*], Ling Shen [b], Jie Ying [a,*], Xiao-Yu Yang [b,*]

[a] School of Chemical Engineering and Technology, Sun Yat-sen University, Zhuhai 519082, China
[b] State Key Laboratory of Advanced Technology for Materials Synthesis and Processing & Shenzhen Research Institute & Joint Laboratory for Marine Advanced Materials in Pilot National Laboratory for Marine Science and Technology (Qingdao), Wuhan University of Technology, Wuhan, 430070, China
[c] Institut für Anorganische Chemie und Strukturchemie, Heinrich-Heine-Universität Düsseldorf, Universitätsstr. 1, D-40225 Düsseldorf, Germany
[d] Hunan University of Technology, Zhuzhou 412007, China

ARTICLE INFO

Keywords:
Nanofused hierarchical porous MIL-101
Morphology control
Dye adsorption
Enhanced catalytic property

ABSTRACT

MIL-101(Cr) can be tailored by using different modulators in the synthesis to obtain several morphological variants, including micro-sized MIL-101(Cr) (M-MIL), nano-sized MIL-101(Cr) (N-MIL) and nanofused hierarchical porous MIL-101(Cr) (H-MIL). Though those MILs had comparable porosity, H-MIL possessed remarkable higher adsorption capacity toward the anionic dye Congo red (CR, 1467 mg/g) and cationic dye methylene blue (MB, 301 mg/g) than the other two samples. Furthermore, in the cyanosilylation reaction, H-MIL also revealed significantly enhanced catalytic activity (yield ~ 95.1%). Thus, the outstanding performance of H-MIL could be attributed to its hierarchically porous structure which accelerated the mass transfer rate and exposed more catalytic active sites.

1. Introduction

Metal-organic frameworks (MOFs) are a sort of novel porous materials with high porosity and rich active sites, which can be single or combined used in the applications of adsorption/separation [1,2], catalysis [3,4], photocatalysis [5–7], energy transformation/storage [8,9], chemical sensing [10,11], hydrogen evolution [12–14] or drug loading [15,16], etc.

MIL-101(Cr), a prototypical Cr-benzenedicarboxylate MOF, has ultrahigh specific surface area (S_{BET} > 4000 m^2/g) and excellent chemical/water stability [17]. Hence, it is most appropriate for applications in response to moisture/water environment, especially in adsorption [18,19] and catalysis fields [20,21]. For instance, Haque et al. reported that MIL-101(Cr) exhibited high adsorption capability for methyl orange (MO) in aqueous solution [22]. Chen et al. found that MIL-101(Cr) was an efficient adsorbent for xylenol orange (XO) [23]. Yang and his group systematically studied the influence of active sites, electrostatic interactions and porosities of MIL-101(Cr) for adsorption of different dyes [24]. Moreover, MIL-101(Cr) was employed as catalysts in many reactions due to its Lewis acid sites [25], such as in the oxidation reaction of long chain olefins [26], indene [27,28] and aryl sulphide [29], etc.

However, the structure and particle sizes of MIL-101(Cr) are crucial to its adsorption capacity and catalytic performance [30]. Though numerous references mentioned the hierarchically porous structured MIL-101(Cr) or nano-sized MIL-101(Cr) could give a higher adsorption efficiency or enhanced catalytic property compared with pristine sample [3,31,32], the systematic comparison of a MOF's capabilities based on various morphological variants are still rare.

Herein, we report the fabrication of different morphological variants of MIL-101(Cr) with micro-crystalline (~1.5 μm), nano-crystalline (~100 nm) size and hierarchically porous (HP) structure (extra-large mesopores ~ 26 nm) via a one-step hydrothermal synthesis. The samples were named as M-MIL, N-MIL and H-MIL, respectively.

In the present work, we carefully investigate the adsorbent property and catalytic performance of the above three MILs. The results demonstrate that H-MIL exhibited the highest adsorption capacity toward the anionic dye Congo red (CR) and cationic dye methylene blue (MB) among the MILs. Furthermore, H-MIL also revealed much higher catalytic activity than the other MILs in the cyanosilylation reaction. These results suggested that, hierarchically the porous structure of MIL-101

Abbreviations: MIL, Materials of Institute Lavoisier.

* Corresponding authors.
E-mail addresses: janiak@hhu.de (C. Janiak), yingj5@mail.sysu.edu.cn (J. Ying), xyyang@whut.edu.cn (X.-Y. Yang).

https://doi.org/10.1016/j.cplett.2022.139859
Received 29 May 2022; Received in revised form 25 June 2022; Accepted 7 July 2022
Available online 8 July 2022
0009-2614/© 2022 Elsevier B.V. All rights reserved.

(Cr) presents significant advantages in adsorption and catalysis applications.

2. Experimental

2.1. Materials

Chromium(III) nitrate nonahydrate ($Cr(NO_3)_3{\cdot}9H_2O$, 99%), benzene-1,4-dicarboxylic acid (H_2bdc, 99%), nitric acid (HNO_3, 65%), sodium hydroxide (NaOH, 99.5%), acetic acid (CH_3COOH, 99.7+%), hydrochloric acid (HCl, ~37%), N,N-dimethylformamide (DMF, 99%), ethanol (CH_3CH_2OH, 99.5%), benzaldehyde (C_7H_6O, 99+%), trimethylsilylcyanide (Me_3SiCN, 97%), heptane (C_7H_{16}, 99%), hexadecane ($C_{16}H_{34}$, 99%). Water with a residual conductivity of 0.1 μS/cm was obtained from a GRO-10L water purification system. All chemicals were purchased from Shanghai Aladdin Biochemical Technology Co., Ltd. and can be used without further purification.

2.2. Synthesis and purification of MIL-101(Cr) samples

M-MIL, N-MIL and H-MIL were obtained by the similar synthetic procedure, the only difference being the use of a different modulator. Generally, 800 mg of $Cr(NO_3)_3{\cdot}9H_2O$ (2 mmol), 332 mg of H_2bdc (2 mmol) and a suitable amount of modulator were dissolved in H_2O. The total volume of the solution was kept as 10 mL. For M-MIL, N-MIL and H-MIL, the added modulator was HNO_3 (1 mmol), NaOH (1 mmol) and CH_3COOH (12 mmol), respectively. The mixture was loaded in a hydrothermal steel autoclave with a Teflon liner, and then placed in an oven and heated up to 220 °C for 8 h. After this time, the oven was cooled down to ambient temperature at the rate of 30 °C/h.

The collected green solid was carefully washed with hot DMF (2 × 30 mL, 70 °C) and CH_3CH_2OH (2 × 30 mL, 60 °C) twice. Then the products were dried in a vacuum oven (120 °C, 1200 Pa, 2 h) and stored for further analysis.

2.3. Characterization

Powder X-ray diffractograms (XRD) were measured on an Ultima IV instrument at ambient temperature using Cu-Kα radiation (λ = 0.1542 nm) at a power of 2 kW with a scan rate of 0.04°/s. N_2 physisorption measurements were carried out at 77 K on a Kubo X1000 instrument. Before the measurement, the samples were degassed for at least 4 h at 120 °C. The morphology of the samples was characterized by scanning electron microscopy (SEM, Nova NanoSEM230) equipped with a W cathode (5 kV) and transmission electron microscopy (TEM, JEM-2100F). UV–vis spectra were collected on a UV-3600 Plus instrument. The zeta potentials were measured on a Zetasizer Nano Z equipment as dispersions in H_2O. The catalytic reaction products were identified and analyzed by using the Agilent Technologies 7890A GC system (Agilent, Palo Alto, CA, USA). All samples were treated and measured under the same conditions.

2.4. Dye adsorption experiments

The concentrations of dyes were detected via UV–vis spectrophotometry at ambient temperature (25 °C). A typical adsorption measurement involves around 5 mg of MILs in dye aqueous solution (50 mL). And the adsorption capability (q_t) of MILs at times t were calculated as follows [33,34]:

$$q_t = \frac{V(c_0 - c_t)}{m} \tag{1}$$

where V (L) stands for the solution volume; c_0 (mg/L) is the beginning concentration of the dyes and c_t (mg/L) is the concentration of the dyes at different times t (min); m (g) is the weight of MILs.

The pseudo-first-order (Eq. (2)) and pseudo-second-order (Eq. (3)) kinetic models are employed to describe the adsorption kinetics of MILs, shown as follows [35]:

$$\ln(q_e - q_t) = \ln q_e - k_1 t \tag{2}$$

$$\frac{t}{q_t} = \frac{1}{k_2 q_e^2} + \frac{t}{q_e} \tag{3}$$

where q_e (mg/g) and q_t (mg/g) are the adsorbed amounts of dyes at equilibrium and time t (min), respectively; k_1 (min^{-1}) and k_2 (g $mg^{-1}min^{-1}$) are the related rate constants.

The Langmuir (Eq. (4)), Temkin (Eq. (5)), and Freundlich (Eq. (6)) isotherm models are used to fit the tested data and their equations are presented as follows [24,35]:

$$\frac{c_e}{q_e} = \frac{c_e}{q_m} + \frac{1}{K_L q_m} \tag{4}$$

$$q_e = B\ln(A) + B\ln c_e \tag{5}$$

$$\ln q_e = \ln K_F + \frac{1}{n}\ln c_e \tag{6}$$

where c_e stands for the dye concentration at equilibrium, q_m (mg/g) is the maximum uptake of adsorbents and K_L (L/mg) is the Langmuir constant; B = (RT/b) is relevant to adsorption heat, A is the Temkin constant; K_F (mg/g) and n are the Freundlich constants.

2.5. Cyanosilylation of benzaldehyde

425 mg (4 mmol) of benzaldehyde, 794 mg (8 mmol) of trimethylsilylcyanide (TMSCN) and 0–20 mg of catalyst (MILs) were added in 15 mL of heptane and 1 mL of hexadecane was used as internal standard. The reaction mixture was stirred at 313 K and the reaction was monitored using an Agilent Technologies 7890A GC system.

3. Results and discussion

3.1. Characterization of MILs

MIL-101(Cr) possesses two sorts of natural pore apertures with the size approx. 12 × 12 Å and 16 × 15 Å, respectively (Fig. S1) [36,37]. In the synthesis procedure of MIL-101(Cr), modulators are commonly used to obtain various structural forms [38–42]. In this work, M-MIL, N-MIL and H-MIL were prepared through involving HNO_3, NaOH and CH_3COOH as modulator, respectively.

The particle sizes and morphologies of MILs are presented in Fig. 1. M-MIL presented the classic octahedral morphology of MIL-101(Cr) with crystal sizes of ~ 1.5 μm, N-MIL possessed a much smaller particle size of approx. 100 nm, while the crystals of H-MIL seemed fused which implied a possible hierarchically porous structure (Fig. 1c-d). The TEM images of H-MIL further confirmed the fusion phenomenon of MIL-101(Cr) crystals, and extra mesopores (15–30 nm) were formed between the fused particles (Fig. 1e-f). The added modulators were of key importance to the crystal growth of MIL-101(Cr). HNO_3 influences the nucleation speed of MIL-101(Cr) and results in micro-sized MIL-101(Cr) crystals [43,44]. On the contrary, NaOH leads to a high pH value and causes a smaller crystal growth rate than the nucleation rate, hence, produces nano-sized MIL-101(Cr) [36,38]. In the case of adding CH_3COOH, the small MIL-101(Cr) crystals are fused together to construct a hierarchical structure, which can be ascribed to the low crystallinity, high surface energy and Ostwald ripening [37,42].

X-ray diffractograms of the MILs are disclosed in Fig. S2. All XRD patterns of the samples were positively matched to the simulated MIL-101(Cr) pattern, which confirmed that the products were pure MIL-101(Cr) (Fig. S2).

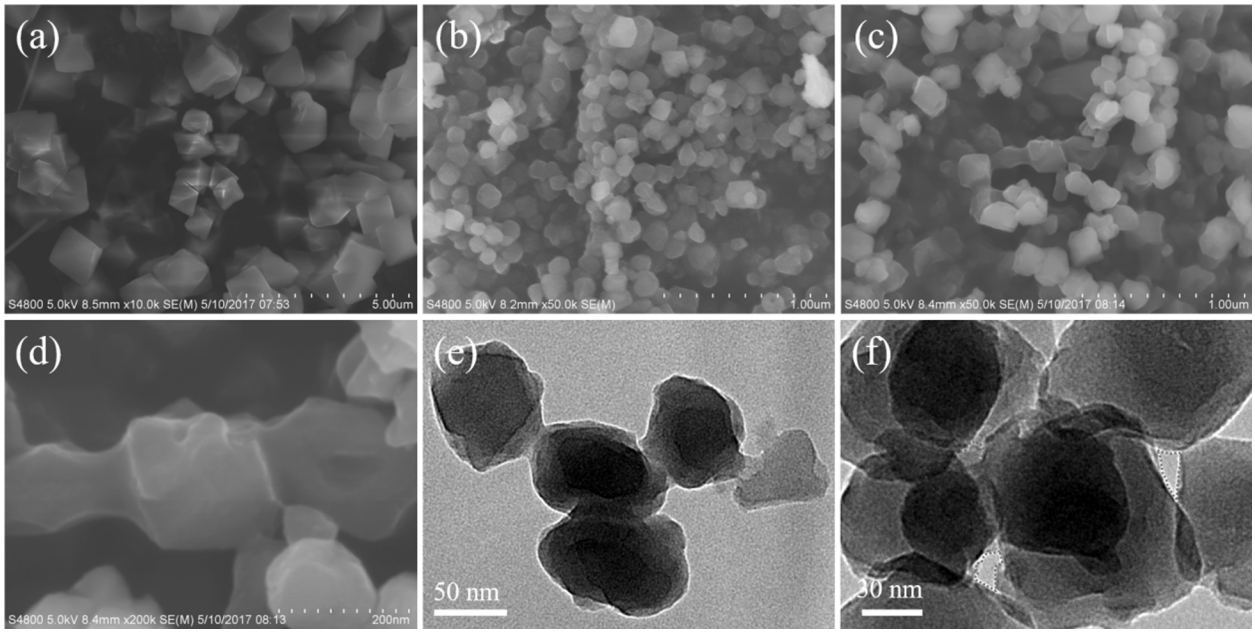

Fig. 1. SEM images of (a) M-MIL, (b) N-MIL and (c-d) H-MIL. (e-f) HRTEM images of H-MIL with different resolution.

N_2 physisorption isotherms, pore size distribution (PSD) curves and volume summary of the MILs were displayed in Fig. 2, and the porous information were summarized in Table 1. M-MIL and N-MIL revealed the classic I(b)-type isotherms (Fig. 2a) [45], which were well in line with the reported literature [17,19]. The N_2 physisorption isotherm of H-MIL was a unique Type IV isotherm with a hysteresis loop in the pressure range of $0.9 < P/P_0 < 0.99$, which was characteristic for (micro-) mesoporous materials (mesopore range from 20 to 30 nm pore diameter) (Fig. 2a) [45]. N-MIL showed the best Brunauer-Emmett-Teller (BET) surface area of 3100 m^2/g, M-MIL and H-MIL had a bit lower porosity with the BET surface area of 2860 m^2/g and 2970 m^2/g, respectively (Fig. 2a, Table 1). The PSD curves and volume summary of MILs were

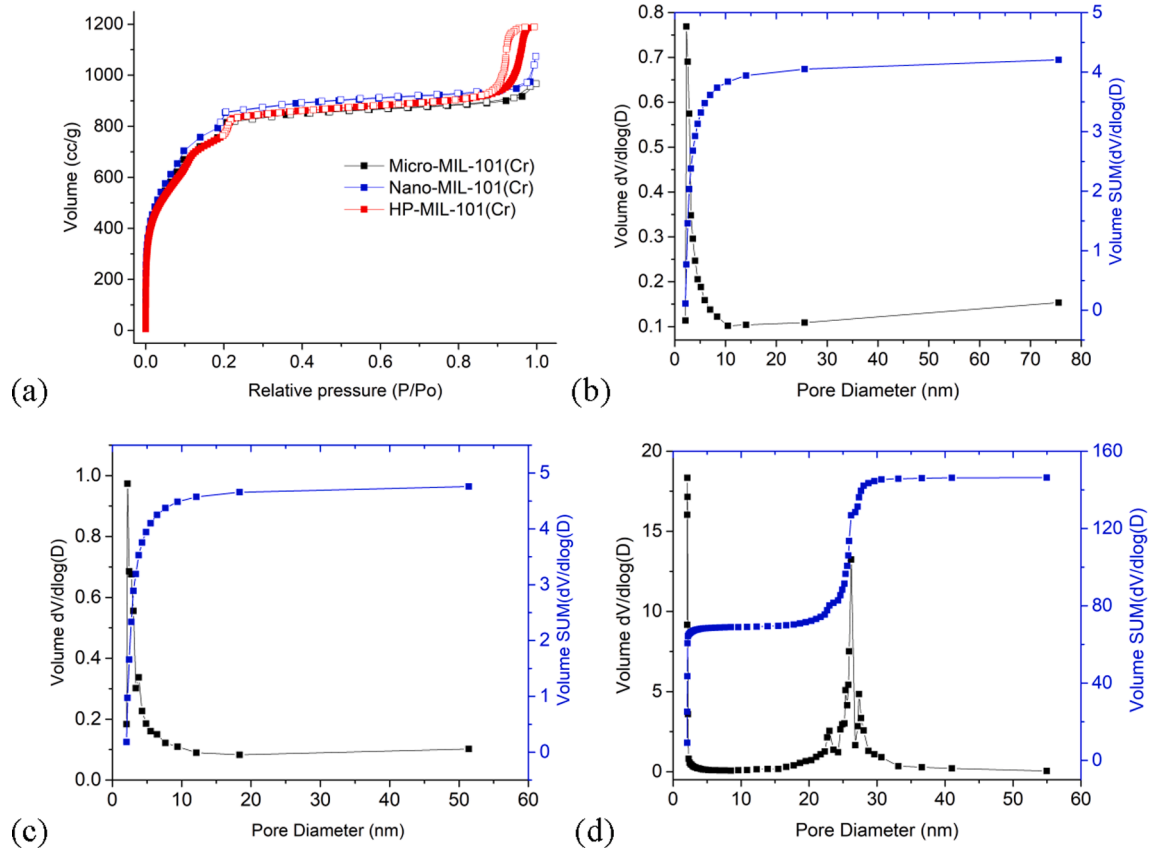

Fig. 2. (a) N_2 physisorption isotherms for MILs. (b)-(d) The pore size distribution curves and volume summary for M-MIL, N-MIL and H- with BJH model, respectively.

Table 1
Porosity information of MIL-101(Cr)s with various additives.

Sample	Yield (%)[a]	S_{BET} (m^2/g)[b]	$S_{Langmuir}$ (m^2/g)	V_{pore} (cm^3/g)[c]
M-MIL	82.5	2860	3930	1.50
N-MIL	43.1	3100	4310	1.66
H-MIL	61.9	2970	4020	1.84

[a] The yield calculation is based on Cr.
[b] All S_{BET} values were determined in the pressure range of $0.05 < p/p_0 < 0.25$.
[c] V_{pore} was calculated from N_2 sorption isotherms at 77 K ($p/p_0 = 0.99$).

disclosed in Fig. 2 (b-d) via Barrett-Joyner-Halenda (BJH) model. Except for the natural micropores of MIL-101(Cr), H-MIL possessed the extra mesopores within 20–30 nm (Fig. 2d), while M-MIL and N-MIL just contained intrinsic micro pores (Fig. 2 b-c). According to the above electron microscopic results, these extra mesopores of H-MIL were formed from the fusion of nano crystals. In this work, the presence of CH_3COOH may cover the MIL-101(Cr) crystal nuclei, decrease the surface crystallinity, raise the surface energy and thereby lead to nano MIL-101(Cr) crystals fused together and form extra mesopores.

3.2. Dyes adsorption of MILs

In order to study the adsorption performances of the MILs, the anionic dye Congo red (CR) and cationic dye methylene blue (MB) were selected as model compounds. At the beginning, the effect of the pH value toward dye adsorption of MILs were tested (Fig. S3). The pH values with optimal adsorption capabilities of CR and MB were 7 and 10, respectively (Fig. S3). Hence, the dye adsorption experiments were conducted at the corresponding optimal pH values.

H-MIL demonstrated the highest uptakes toward CR and MB among the MILs, with the maximum value of 1467 mg/g and 301 mg/L, respectively (Fig. 3a, b). Especially for CR, the uptake of H-MIL was significantly higher than that of other adsorbents which were reported in recent years (Table S1) [46–53]. M-MIL and N-MIL, however, showed markedly lower CR adsorption of 1034 mg/g and 1295 mg/g, respectively, though all MILs presented comparable specific surface areas (Table 1). While for MB, the results were quite different, only H-MIL exhibited a good adsorption capacity of 301 mg/g, M-MIL and N-MIL essentially cannot adsorb MB (Fig. 3b). Undoubtably, the adsorption capabilities of the MILs were not only related to their own structures, but also related to dye characteristics. The structures of CR and MB are presented in Fig. S4, CR is an anionic dye, whereas MB is cationic. The CR molecule possessed more aromatic rings than that of the MB molecule. Thus, π-π interactions between the CR and MILs were stronger than that of MB and MILs, which may induce higher uptakes of MILs toward CR.

Additionally, the electrical properties of the obtained MILs were also measured by zeta potentiometry. The zeta potentials of the MIL crystallites were 23.0 mV, 18.3 mV and 1.79 mV for M-MIL, N-MIL and H-MIL, respectively (Fig. S5). Therefore, the surfaces of the three MILs were covered with positive charges, however, the zeta potential of H-MIL was much lower compared with M-MIL and N-MIL. Thus, for the cationic dye MB, only H-MIL disclosed appreciable adsorption capability, while the more positively charged M-MIL and N-MIL showed nearly no adsorption for MB. On the contrary, positive charges favored the adsorption of the negative charged anionic dye, hence, all MILs demonstrated higher uptakes for CR. Moreover, H-MIL possessed unique hierarchical pores, which raised the accessibility of the adsorbent and accelerated the mass transport of dyes. This largely enhanced the adsorption capacity of the porous material, especially for large dye molecules [54,55]. All in all, H-MIL showed significant advantages in dye adsorption, including both the anionic dye Congo red and the cationic dye methylene blue.

The time-dependent adsorption capabilities of MILs for dyes were also investigated, as shown in Fig. 3 (c, d). And the adsorption kinetics curves which were fitted with Eqs. (2) and (3) were displayed in Fig. 3 (e-h), the corresponded parameters were listed in Table S2. Obviously, the R^2 values of the pseudo-second order kinetics model were much higher than those of the pseudo-first order model, and the theoretical equilibrium adsorption capability, theoretical q_e, was highly consistent with the test value (Table S2). Thus, it implied that the pseudo-second order procedure was dominating for both CR and MB adsorption experiments. According to the intraparticle diffusion model, the plot of adsorption capability (q_t) versus the square root of time ($t^{1/2}$) should be linear [56]. However, in our experiments, all dye plots were not linear (Fig. S6), which indicated that the adsorption of MILs for CR and MB contained multiple stages and the intraparticle transport was not the rate-limiting step.

We note that the equilibrium rate, that is the uptake of CR versus time after about 40 min in Fig. 3c becomes very similar. This is to be expected as the filling of the MOF pores will slow down the adsorption rate asymptotically towards zero with similar rates after a certain time. However, the initial rate between 0 and 10 min is quite different. In this time window, the rate q_t/10 min increases from 29.1 mg/(g min) for M-MIL, 30.9 mg/(g min) for N-MIL to 34.2 mg/(g min) for H-MIL. It is this initial rate to which we refer in terms of better mass transport.

The zeta potential should have played a role on the adsorption rate. However, from Fig. S5 it is evident that the positive zeta potential decreases from M-MIL over N-MIL to H-MIL, which is opposite to the rate increase seen for the uptake of the negative dye CR. Thus, H-MIL has the lowest positive zeta potential of only ~+1.8 mV but the fastest initial uptake rate. This speaks against a decisive role of the zeta potential on the initial adsorption rate.

In the interest of assessing the adsorption performance and calculating the maximum adsorption capabilities of the MILs for dyes, the Langmuir, Temkin, and Freundlich isotherm models were employed to fit the test data (the models were described in the Exp. Part). Fig. 4 revealed the equilibrium adsorption isotherms for CR, and MB, and the related fitting parameters were listed in Table S3. For all adsorptions, the experimental data were highly in line with the Langmuir isotherm model, and the correlation regression coefficients of R^2 were over 0.99, which were much higher than that of Temkin and Freundlich models (Fig. 4, Table S3). Especially, in the case of adsorption of MB, the equilibrium isotherms were poorly fitted with the Temkin and Freundlich models in the range of 50–500 mg/L, but matched very well with the Langmuir model (Fig. 4, Table S3). Moreover, for the Langmuir model, the theoretical maximum uptakes of the MIL-101(Cr) samples toward all dyes were in good agreement with the experimental data (Table S3).

The reusability of the MIL adsorbent will be important for the industrial utilization. Thus, the regeneration of H-MIL was studied by using ethanol, CH_3CH_2OH as an extracting agent. Four successive adsorption-desorption cycles were conducted, and the adsorption capability of H-MIL for CR and MB reduced<10%, indicating that H-MIL possessed good reusability for dye adsorption (Fig. S7). Moreover, XRD disclosed that structure of H-MIL was the same after four successive adsorption-desorption cycles (Fig. S8).

3.3. Catalytic performance of MILs

In order to evaluate the catalytic activity of MIL-101(Cr), the cyanosilylation of aldehydes was employed as a test reaction catalyzed by Lewis acids (Fig. S9). In fact, aldehydes or ketones were promptly converted into the relevant cyanohydrin trimethylsilyl ethers in the presence with cyanotrimethylsilane by involving Lewis acids as catalyst. As early as 1994, a 2D network compound $[Cd(4,4'\text{-bpy})_2](NO_3)_2$ was synthesized and used as catalyst in the cyanosilylation of aldehydes [57]. Then, Kaskel and the coworkers reported that the dehydrated HKUST-1 (a Cu-benzene-1,3,5-tricarboxylate MOF) showed relatively good catalytic capacity in the cyanosilylation of aldehydes with a yield of ~ 57% after 3 days at 40 °C [58].

In this work, a series of experiments were carried out based on

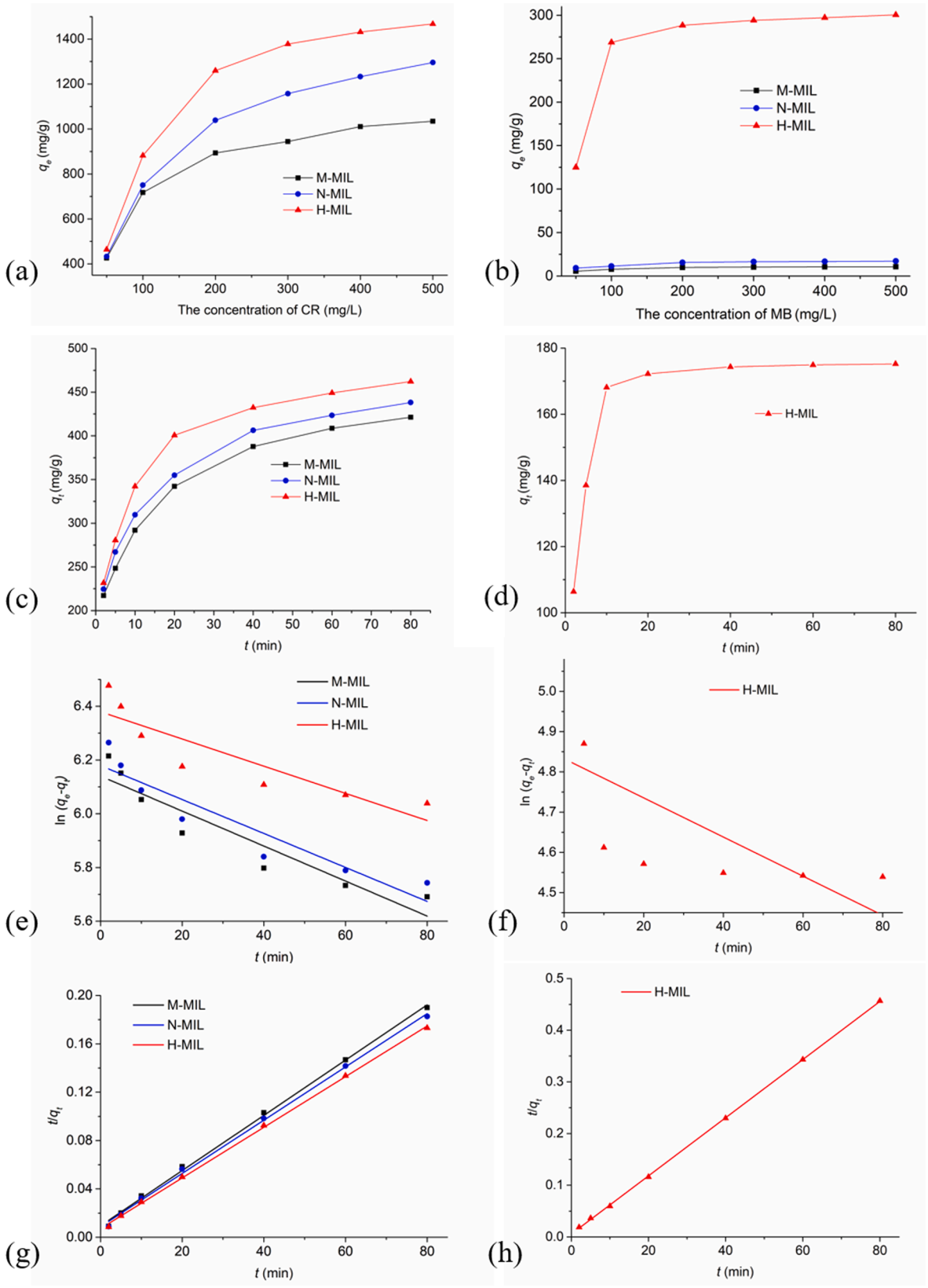

Fig. 3. Adsorption capabilities of MILs toward the various dyes after 24 h, as measured by dispersing 5 mg of MILs in the aqueous solution (50 mg/L to 500 mg/L) at 25 °C. (a) CR, (b) MB; The effect of adsorption time on (c) CR and (d) MB adsorption capability for MILs; Fitting results of dyes on MILs by using (e, f) pseudo-first-order kinetic and (g, h) pseudo-second-order kinetic. (e, g) CR, (f, h) MB.

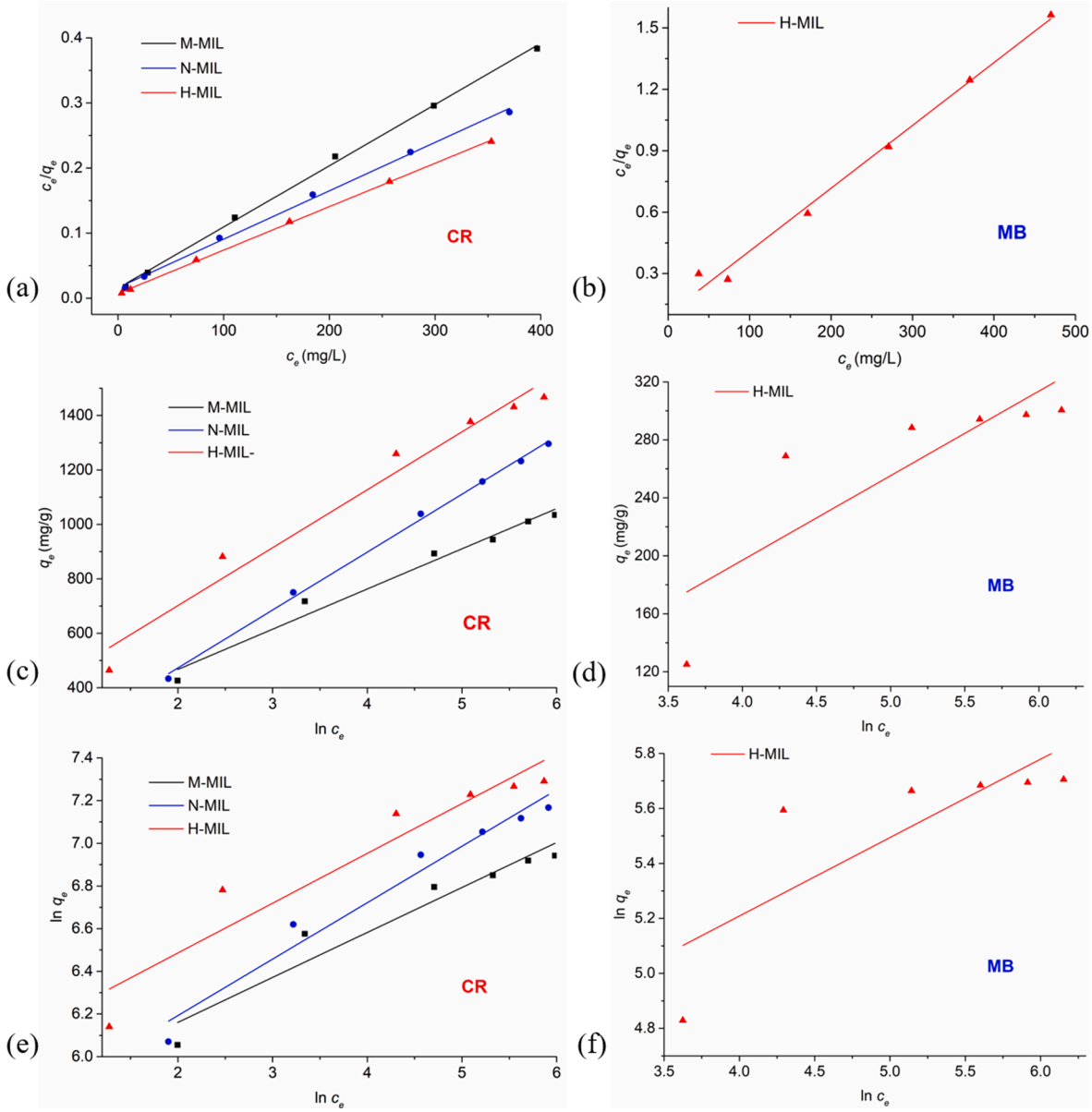

Fig. 4. Fitting results of dye adsorption on MILs by using (a-b) Langmuir, (c-d) Temkin and (e-f) Freundlich isotherm models.

various amounts of MILs to optimize the catalytic reaction condition, and the analyzed results were disclosed in Table 2. It was found that as the amount of MILs increased, the yield also increased accordingly, but when the weight of the MILs was over 10 mg, the yield increase was rather limited (Table 2). Furthermore, H-MIL exhibited much higher catalytic capability compared with the other two samples under the same condition (Fig. 5a). For instance, after 120 min, the yield of the reaction for H-MIL was 95.1% (20 mg), while for M-MIL and N-MIL it was only 68.6% (20 mg) and 79.9% (20 mg), respectively (Fig. 5a, Table 2). In the present work, the average reaction rate of H-MIL (20 mg, 120 min) was 95.1 mmol·g^{-1}·h^{-1}, which was much higher than that of M-MIL (68.6 mmol·g^{-1}·h^{-1}) and N-MIL (79.9 mmol·g^{-1}·h^{-1}) (average reaction rate of the catalyst = (mol of product)/(mass of catalyst × reaction time)). Additionally, H-MIL revealed quite good reusability during the tests. After 3 cycles, the product yield still achieved ~ 85% (Fig. 5b). While for M-MIL and N-MIL, after 3 cycles, both of the product yields were below 50% (Fig. 5b).

Table 2
The yields (%) of the cyanosilylation of aldehyde reaction by MILs with different weights after 120 min of the reaction.

Sample	0 mg	5 mg	10 mg	15 mg	20 mg
M-MIL	0%	58.5%	64.8%	67.4%	68.6%
N-MIL	0%	71.4%	76.3%	79.2%	79.9%
H-MIL	0%	88.3%	92.5%	94.7%	95.1%

The plausible mechanism of enhanced catalytic capability and reusability of H-MIL may be contributed to its unique nanofused hierarchical pores. On one hand, the hierarchical structure could facilitate mass transfer, increase the accessibility of inner active sites, especially in terms of macromolecules, thus, H-MIL would accelerate both reactant and product transfer in the reaction progress and speed up the reaction [3,55,59]. On the other hand, the larger nanofused mesopores are less likely to be blocked by reactants and generated products [2,55,60], hence, H-MIL possessed good reusability in the cyanosilylation of aldehydes.

4. Conclusions

In conclusion, compared with M-MIL and N-MIL, H-MIL presented a

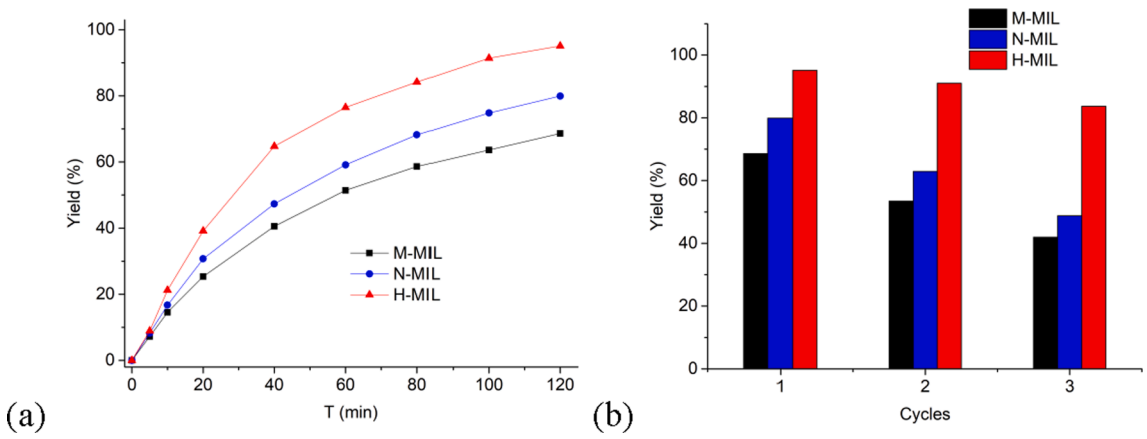

Fig. 5. (a) Time-dependent yield of the cyanosilylation of aldehyde reaction in the presence of MILs. Comparison of the yields for MILs over 3 reaction runs (120 min, 20 mg).

remarkable higher adsorption capacity for CR (1467 mg/g) and MB (301 mg/g). Additionally, H-MIL also showed a significant enhancement of catalytic performance (yield > 95%) in the cyanosilylation of aldehydes. The outstanding performance of H-MIL could be attributed to its unique nanofused hierarchical structure. Hence, it will help us to better understand the mechanism of organic dye adsorption and catalysis by MOFs, and contiguously enlarge the utilization in practical fields.

CRediT authorship contribution statement

Tian Zhao: Conceptualization, Formal analysis, Writing – original draft. **Wei Geng:** Methodology. **Ming Dong:** Investigation. **Yi Zhao:** Formal analysis. **Christoph Janiak:** Resources, Supervision, Writing – review & editing. **Ling Shen:** Data curation. **Jie Ying:** Resources, Review & editing. **Xiao-Yu Yang:** Supervision, Resources.

Declaration of Competing Interest

The authors declare that they have no known competing financial interests or personal relationships that could have appeared to influence the work reported in this paper.

Acknowledgements

The work was supported by the National Natural Science Foundation of China (51802094, 52002414, 51861135313), Guangdong Basic and Applied Basic Research Foundation (2019A1515110436, 2019A1515110590), Sino-German Centre's COVID-19 Related Bilateral Collaborative project (C-0046) Guangzhou Science and Technology Project (202102020463), the Science and Technology Program of Hunan Province, China (2018RS3084), Guangdong Province International Scientific and Technological Cooperation Projects (2020A0505100036), International Science & Technology Cooperation Program of China (2015DFE52870), Guangdong Basic and Applied Basic Research Foundation (2022A1515010137), Shenzhen Science and Technology Program (JCYJ20210324142010029), National 111 project (B20002), and Program for Changjiang Scholars and Innovative Research Team in University (IRT_15R52). CJ thanks the Deutsche Forschungsgemeinschaft (DFG) for grant 396890929/GRK 2482.

References

[1] S. Qiu, J. Du, Y. Xiao, Q. Zhao, G. He, Sep. Purif. Technol. 271 (2021) 118868.
[2] D. Liu, D. Zou, H. Zhu, J. Zhang, Small 14 (2018) e1801454.
[3] Y. Shen, T. Pan, L. Wang, Z. Ren, W. Zhang, F. Huo, Adv. Mater. 33 (2021) 2007442.
[4] L. Ma, C. Abney, W. Lin, Chem. Soc. Rev. 38 (2009) 1248.
[5] X. Liu, Y. Hou, M. Tang, L. Wang, Chin. Chem. Lett. (2022).
[6] L. Wang, L. Xie, W. Zhao, S. Liu, Q. Zhao, Chem. Eng. J. 405 (2021) 127028.
[7] X. Cheng, L. Wang, L. Xie, C. Sun, W. Zhao, X. Liu, Z. Zhuang, S. Liu, Q. Zhao, Chem. Eng. J. 439 (2022) 135757.
[8] R. Banerjee, A. Phan, B. Wang, C. Knobler, H. Furukawa, M. O'Keeffe, O.M. Yaghi, Science 319 (2008) 939.
[9] Z.-J. Zheng, H. Ye, Z.-P. Guo, Energy Environ. Sci. 14 (2021) 1835.
[10] G. Chakraborty, I.H. Park, R. Medishetty, J.J. Vittal, Chem. Rev. 121 (2021) 3751.
[11] M. Ding, X. Cai, H.L. Jiang, Chem. Sci. 10 (2019) 10209.
[12] L. Xie, L. Wang, W. Zhao, S. Liu, W. Huang, Q. Zhao, Nature Commun. 12 (2021).
[13] S. Wang, L. Wang, L. Xie, W. Zhao, X. Liu, Z. Zhuang, Y. Zhuang, J. Chen, S. Liu, Q. Zhao, Nano Res. 15 (2022) 4996.
[14] J. Chen, Y. Tang, S. Wang, L. Xie, C. Chang, X. Cheng, M. Liu, L. Wang, L. Wang, Chin. Chem. Lett. 33 (2022) 1468.
[15] X. Zhang, Z. Chen, X. Liu, S.L. Hanna, X. Wang, R. Taheri-Ledari, A. Maleki, P. Li, O.K. Farha, Chem. Soc. Rev. 49 (2020) 7406.
[16] Y. Wei, T.E. Parmentier, K.P. de Jong, J. Zecevic, Chem. Soc. Rev. 44 (2015) 7234.
[17] G. Ferey, C. Mellot-Draznieks, C. Serre, F. Millange, J. Dutour, S. Surble, I. Margiolaki, Science 309 (2005) 2040.
[18] W. Xu, W. Li, L. Lu, W. Zhang, J. Kang, B. Li, J. Solid State Chem. 279 (2019) 120950.
[19] B. Tan, Y. Luo, X. Liang, S. Wang, X. Gao, Z. Zhang, Y. Fang, Ind. Eng. Chem. Res. 58 (2019) 2983.
[20] S. Bernt, V. Guillerm, C. Serre, N. Stock, Chem. Commun. (Camb.) 47 (2011) 2838.
[21] S. Oudi, A.R. Oveisi, S. Daliran, M. Khajeh, E. Teymoori, J. Colloid Interface Sci. 561 (2020) 782.
[22] E. Haque, J.E. Lee, I.T. Jang, Y.K. Hwang, J.S. Chang, J. Jegal, S.H. Jhung, J. Hazard. Mater. (2010) 535.
[23] C. Chen, M. Zhang, Q. Guan, W. Li, Chem. Eng. J. 183 (2012) 60.
[24] W. Zhang, R.-Z. Zhang, Y.-Q. Huang, J.-M. Yang, Crystal Growth Des. 18 (2018) 7533.
[25] A. Santiago-Portillo, S. Navalón, P. Concepción, M. Álvaro, H. García, ChemCatChem 9 (2017) 2506.
[26] J. Ying, A. Herbst, Y.X. Xiao, H. Wei, G. Tian, Z. Li, X.Y. Yang, B.L. Su, C. Janiak, Inorg. Chem. 57 (2018) 899.
[27] T. Zhao, M. Dong, L. Yang, Y. Liu, Catalysts 8 (2018) 394.
[28] T. Zhao, J. Yu, Z. He, N. He, M. Dong, Z. Chen, H. Chen, Nanosci. Nanotechnol. Lett. 11 (2019) 229.
[29] Y.K. Hwang, D.-Y. Hong, J.-S. Chang, H. Seo, M. Yoon, J. Kim, S.H. Jhung, C. Serre, G. Férey, Appl. Catal. A: General 358 (2009) 249.
[30] M.Y. Zorainy, M. Gar Alalm, S. Kaliaguine, D.C. Boffito, J. Mater. Chem. A 9 (2021) 22159.
[31] Y. Hara, K. Sakaushi, Nanoscale 13 (2021) 6341.
[32] G. Cai, P. Yan, L. Zhang, H.C. Zhou, H.L. Jiang, Chem. Rev. 121 (2021) 12278.
[33] Q. Liu, H. Yu, F. Zeng, X. Li, J. Sun, X. Hu, Q. Pan, C. Li, H. Lin, Z. min Su, J. Colloid Interface Sci. 579 (2020) 119.
[34] Q. Liu, S. Li, H. Yu, F. Zeng, X. Li, Z. Su, J. Colloid Interface Sci. 561 (2020) 211.
[35] X.-L. Li, W. Zhang, Y.-Q. Huang, Q. Wang, J.-M. Yang, Colloids Surf. Physicochem. Eng. Aspects 619 (2021) 126549.
[36] T. Zhao, S.-H. Li, L. Shen, Y. Wang, X.-Y. Yang, Inorg. Chem. Commun. 96 (2018) 47.
[37] T. Zhao, L. Yang, P. Feng, I. Gruber, C. Janiak, Y. Liu, Inorg. Chim. Acta 471 (2018) 440.
[38] N.A. Khan, I.J. Kang, H.Y. Seok, S.H. Jhung, Chem. Eng. J. 166 (2011) 1152.
[39] D. Jiang, A.D. Burrows, K.J. Edler, Crystengcomm 13 (2011) 6916.
[40] T. Shen, J. Luo, S. Zhang, X. Luo, J. Environ. Chem. Eng. 3 (2015) 1372.
[41] L. Yang, T. Zhao, I. Boldog, C. Janiak, X.Y. Yang, Q. Li, Y.J. Zhou, Y. Xia, D.W. Lai, Y.J. Liu, Dalton Trans 48 (2019) 989.
[42] T. Zhao, S. Li, Y.-X. Xiao, C. Janiak, G. Chang, G. Tian, X.-Y. Yang, Sci. China-Mater. 64 (2021) 252.
[43] T. Zhao, F. Jeremias, I. Boldog, B. Nguyen, S.K. Henninger, C. Janiak, Dalton Trans 44 (2015) 16791.

[44] T. Zhao, H. Zhu, M. Dong, Catalysts 10 (2020) 318.
[45] M. Thommes, K. Kaneko, A.V. Neimark, J.P. Olivier, F. Rodriguez-Reinoso, J. Rouquerol, K.S.W. Sing, Pure Appl. Chem. 87 (2015) 1051.
[46] M.K. Purkait, A. Maiti, S. DasGupta, S. De, J. Hazard. Mater. 145 (2007) 287.
[47] A. Zaghloul, A.A. Ichou, M. Abali, R. Benhiti, A. Soudani, G. Carja, M. Chiban, M. Zerbet, F. Sinan, Biointerface Res. Appl. Chem. 11 (2021) 14986.
[48] V. Srivastava, A.K. Choubey, J. Mol. Struct. 1242 (2021) 130749.
[49] Q. Wang, Y. Zhao, Z. Shi, X. Sun, T. Bu, C. Zhang, Z. Mao, X. Li, L. Wang, Chem. Eng. J. 420 (2021) 129955.
[50] X. Wu, J. Xiong, S. Liu, J.-H. Cheng, M.-H. Zong, W.-Y. Lou, J. Hazard. Mater. 417 (2021) 126011.
[51] R. Xu, H. Du, C. Liu, H. Liu, M. Wu, X. Zhang, C. Si, B. Li, J. Clean. Prod. 313 (2021).
[52] W. Chen, Z. Liu, Q. Tang, B. Du, X. Huang, Y. Mo, L. Fan, H. Luo, F. Chen, J. Environ. Manage. 293 (2021).
[53] S. Anuma, P. Mishra, B.R. Bhat, J. Hazard. Mater. 416 (2021) 125929.
[54] F. Lorignon, A. Gossard, M. Carboni, Chem. Eng. J. 393 (2020) 124765.
[55] L. Feng, K.Y. Wang, X.L. Lv, T.H. Yan, H.C. Zhou, Natl Sci Rev 7 (2020) 1743.
[56] R. Gong, J. Ye, W. Dai, X. Yan, J. Hu, X. Hu, S. Li, H. Huang, Ind. Eng. Chem. Res. 52 (2013) 14297.
[57] M. Fujita, Y.J. Kwon, S. Washizu, K. Ogura, J. Am. Chem. Soc. 116 (1994) 1151.
[58] A. Henschel, K. Gedrich, R. Kraehnert, S. Kaskel, Chem. Commun. (Camb.) (2008) 4192.
[59] H.V. Doan, H. Amer Hamzah, P. Karikkethu Prabhakaran, C. Petrillo, V.P. Ting, Nanomicro Lett 11 (2019) 54.
[60] H.-Y. Guan, R.J. LeBlanc, S.-Y. Xie, Y. Yue, Coord. Chem. Rev. 369 (2018) 76.